Q. J. R. Meteorol. Soc. (2003), **129**, pp. 1989–2010 doi: 10.1256/qj.02.133

Improvements to the representation of orography in the Met Office Unified Model

By S. WEBSTER*, A. R. BROWN, D. R. CAMERON and C. P. JONES
Met Office, UK

(Received 14 June 2002; revised 22 November 2002)

SUMMARY

Three improvements to the representation of orography for use in numerical weather- and climate-prediction models are presented. The first improvement is to replace the US Navy dataset with a new digitally generated dataset as the definition of the true earth topography. There are large differences on all scales between the two datasets and these lead to large differences in the mean and subgrid-scale fields that are derived from them. The second improvement is to filter the mean and subgrid-scale orography (SSO) fields to remove grid-scale and near-grid-scale features and thus suppress forcing on scales that the model cannot treat well. The third improvement is to implement a new, simple parametrization of the effects of SSO in which the total surface pressure drag is calculated using the analytical expression for linear hydrostatic flow over a two-dimensional ridge in the absence of friction and rotation. The surface pressure drag is partitioned into gravity-wave and blocked-flow components that depend on the Froude number of the flow impinging on the SSO. The new scheme attributes about 70% of the total drag to flow blocking.

These improvements have been incorporated into a new version of the Met Office Unified Model. A series of numerical weather-prediction experiments demonstrates that the introduction of the new SSO scheme is the most significant change. In particular, significant improvements to forecast skill, attributable to the SSO scheme's flow-blocking drag component, are found at low levels in the northern hemisphere and the Tropics for an extended northern hemisphere wintertime forecast trial. Furthermore, there are no significant degradations in skill at upper levels, in the southern hemisphere or for summertime trials.

KEYWORDS: Flow blocking Gravity-wave drag Parametrization Smoothing

1. INTRODUCTION

The representation of orography has long been known to be crucial to the performance of global circulation models (GCMs). Palmer *et al.* (1986) and McFarlane (1987) were the first to show clearly the benefits of augmenting the resolved GCM orography with a represention of the effects of subgrid-scale orography (SSO). This they did by using a gravity-wave-drag (GWD) parametrization that accounted for the drag induced by the breaking or absorption of linear hydrostatic gravity waves excited by air flowing over the SSO. Typically, most of the drag applied by these original GWD schemes was exerted in the lower stratosphere.

More recently, further improvements in the representation of the effects of SSO have been made by additionally accounting for various tropospheric SSO drag mechanisms. Thus, as described in Gregory *et al.* (1998, hereafter GSM98), the SSO scheme used in the old version of the Met Office Unified Model (UM) from January 1995 until August 2002 (hereafter the 95 scheme) includes a representation of tropospheric GWD due to hydraulic jumps and trapped lee waves, whilst at low levels a representation of the impact of SSO on boundary-layer drag is also included. Elsewhere, Lott and Miller (1997, hereafter LM97) have shown that the numerical weather-prediction performance of a similar configuration, but without hydraulic jumps, was significantly improved by including an explicit low-level flow-blocking scheme. More recently, Scinocca and McFarlane (2000, hereafter SM00) have shown the benefit of including a flow-blocking scheme in their global climate simulations. Thus, the absence of a flow-blocking scheme in the 95 scheme described previously appears to be a distinct weakness. One of the

* Corresponding author: Met Office, London Road, Bracknell, Berkshire RG12 2SZ, UK.
e-mail: stuart.webster@metoffice.com

main aims of this paper is therefore to present a new UM SSO scheme that includes a flow-blocking component. The new scheme is very simple, with the predicted drag essentially being an empirical fit to the idealized simulations of Ólafsson and Bougeault (1997, hereafter OB97) that include friction and rotation.

At the Met Office a new version of the UM has been used in operational forecast runs since 7 August 2002. The new version of the UM is built around a new dynamical core and includes improvements to many aspects of the model physics. Thus, the new SSO scheme is just one of many developments that have been implemented in the new model. Two other significant changes to the representation of orography have also been implemented in the new model. The first is to replace the US Navy dataset with a new, more accurate 'Global Land One kilometre Base Elevation' dataset (GLOBE) (GLOBE Task team *et al.* 1999). The second is to smooth the (resolved) mean orography to inhibit the forcing of grid-scale numerical noise which, in recent years, has increasingly caused problems in the UM.

The structure of this paper is as follows. Sections 2–4 in turn describe the use of the GLOBE dataset, the grid-scale filtering and the SSO scheme, while section 5 describes the new version of the UM. The numerical weather-prediction trials used to investigate the impact of the changes of sections 2–4, both individually and as a whole, are then described in section 6 before a summary in section 7.

2. The new orography dataset

The old global orography dataset, which was manually derived by the US Navy in the mid-1970s from the best contemporary contour maps, has a resolution of $10'$ which equates to a resolution of about 20 km on the earth's surface. The version used at the Met Office also includes an improved dataset for Antarctica which was supplied by the British Antarctic Survey, correcting gross errors in the Antarctic elevations in the original Navy dataset. The new orography dataset is known as GLOBE and has a resolution of $30''$ which equates to a resolution of about one kilometre. This dataset has been digitally generated and is arguably the best global dataset currently freely available.

In this paper, with the exception of the fields derived for use by the boundary-layer scheme, the resolution of the GLOBE dataset has been reduced to that of the Navy dataset by calculating the arithmetic mean of the $30''$ data for each $10'$ resolution grid cell. In the first instance this reduction in resolution was motivated by the computational limitations of processing such a large dataset. Averaging the GLOBE dataset up in this way obviously also allows a simple direct comparison of the two datasets. However, this averaging acts as a filter on the data and completely removes all scales smaller than 40 km. This filtering is not very scale selective though and so scales longer than 40 km will also be damped. Thus, the averaging procedure may reject a large amount of useful information and hence have a significant impact on the characterization of the SSO. Indeed, SM00 found that retaining the correct scales in the data was very important to the calculation of the anisotropy of the SSO. They found that retaining scales less than 20 km led to an arguably unrealistic reduction in the anisotropy. As shown by GSM98, the anisotropy is a key input to the SSO scheme so it is obviously important to use an optimal description. We hope soon to overcome the computational limitations of processing the GLOBE dataset, and therefore be able to apply a scale-selective filter to the $30''$ data to remove those scales that diminish the anisotropy while not adversely affecting the longer scales that are important in describing the anisotropy.

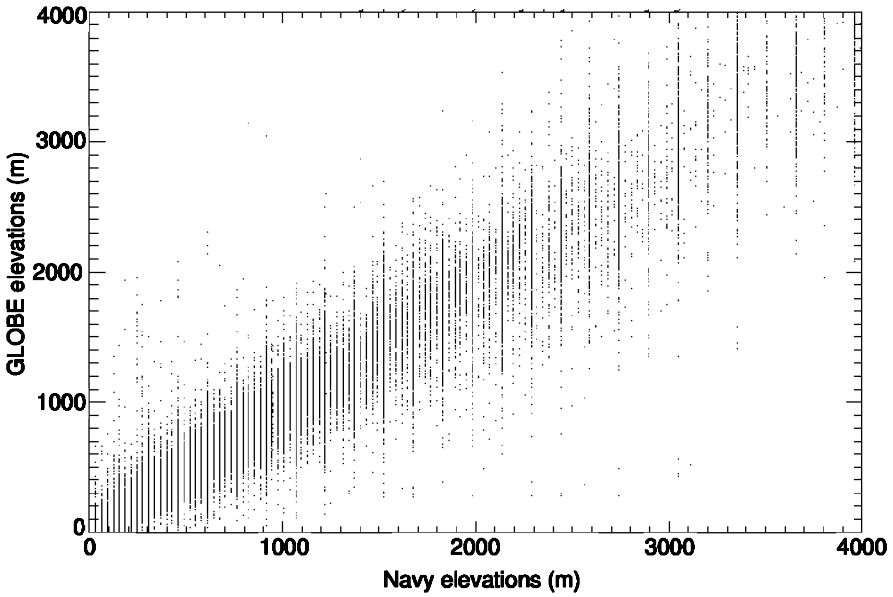

Figure 1. Scatter diagram of the elevations of the GLOBE dataset plotted against those of the Navy dataset. Only points in the rectangular domain bounded by (0°E, 0°N) in its south-west corner and (90°E, 50°N) in its north-east corner have been plotted.

(*a*) *Differences between the GLOBE and Navy datasets*

The most striking difference between the two datasets is illustrated in Fig. 1, which plots the elevations of the GLOBE dataset against the corresponding elevations of the Navy dataset for a region of the northern hemisphere. The feature to note is the equispaced vertical striping. The Navy data is restricted to a discrete set of values whilst the GLOBE data values are essentially continuous. The spacing of the stripes is actually 500 feet (152.4 m), the contour interval of the contour maps used to create the Navy dataset. These stripes imply a significant difference between the datasets at the smallest scales, with the Navy dataset containing much more power at this scale than the GLOBE one.

A further illustration of the differences between the two datasets is given in Fig. 2, where the topmost two lines compare the elevations along the southern edge of the Tibetan Plateau. Large differences are apparent on even the broadest scales, with the GLOBE orography about one kilometre lower around 85°E (the Himalayas region), for example. Structures that look unrealistic are evident at the smallest scales of the Navy dataset. For instance, again at 85°E, the heights jump back and forth twice between two values to exhibit an unrealistic 'sawtooth' pattern. Even on the global scale, the two datasets differ significantly. For example, the global mean elevation for the GLOBE dataset is 233 m, whilst for the Navy dataset it is 235 m.

Given its evident superiority over the US Navy dataset, significant improvements in the modelled orography response might be expected when moving to use the GLOBE dataset.

(*b*) *Impacts on the orography fields input into the UM*

The change in dataset will change the resolved and SSO fields used by the UM. In addition to the source dataset elevations discussed in the previous subsection,

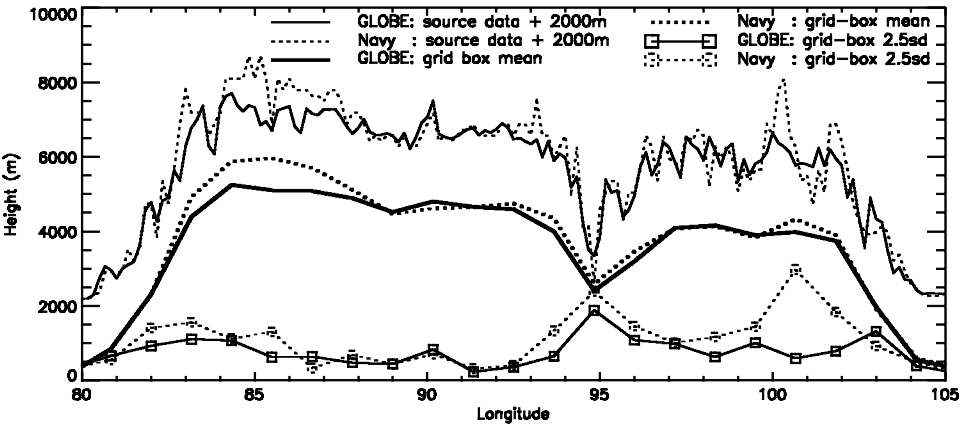

Figure 2. Cross-section along 29°N through the Himalayas comparing the GLOBE dataset (solid lines) with the Navy dataset (dashed lines). The GLOBE source dataset has been averaged up to the same 10′ resolution as that of the Navy source dataset. In the key sd stands for standard deviation. Note that 2000 m has been added to the source data curves to separate them from the grid-box mean curves. The units of longitude are degrees.

Fig. 2 also shows the mean and the 2.5σ fields for the two datasets (where σ is the standard deviation of the SSO and, as we shall describe in section 4, 2.5σ is taken by the new SSO scheme to be the height of the highest SSO peaks above the mean orography). These two fields were calculated assuming that the grid box has a grid spacing six times that of the source datasets, as used in the forecast tests of section 6. The differences in the source datasets already mentioned are evident in the mean and the 2.5σ fields. Thus, in general, both these fields are reduced with the GLOBE dataset. Locally, these reductions can be very large with, for example, the mean orography about 1 km lower around 85°E and the 2.5σ field reduced by a factor of 4 close to 101°E.

The change in dataset also has a large impact on the description of the five other orography fields used by the UM. Three of these describe the anisotropy of the SSO and are, following the notation of GSM98, referred to as the σ_{xx}, σ_{xy} and σ_{yy} fields, and are the grid-box average squared gradients of the source dataset (e.g. $\sigma_{xx} = (\partial h_s(x, y)/\partial x)^2$, where h_s is the height of the source dataset). These fields are typically a factor of 2 larger when calculated from the Navy dataset. This is a result of the spurious power at the smallest scales in this dataset. As described in section 4(c), the drag predicted by the SSO scheme is directly proportional to these fields and so, to keep the predicted drag broadly the same, the change in dataset requires a factor of 2 change in the amplitude of the SSO response (by changing the wave-number constant $\widehat{K}^{-1}$). The remaining two fields input to the UM describe the orography on the smallest scales and are input to the boundary-layer orographic roughness scheme (see GSM98 and Mason (1985) for more details of this scheme and the motivation behind it). They are the A/S field, which is the frontal area A of the SSO per unit horizontal area S, and the peak to trough height field (hereafter P-T-H), which is defined as $2\sqrt{2}\sigma_h$, where σ_h is the standard deviation of the GLOBE dataset at 30″ resolution or the standard deviation of the 10′ resolution Navy dataset (σ_h and σ are therefore the same for the Navy dataset). Ideally, both these fields should be calculated from a very high-resolution dataset, of the order of 100 m resolution. The σ_h field is relatively insensitive to the resolution of the source data so this field is used unmodified. In contrast, the A/S field is very sensitive to the resolution of the source data and so an alternative approach for generating this

field is required for both datasets. For the Navy dataset, this field was generated by calculating A/S from a $3''$ resolution dataset covering Europe and then performing a linear regression of the resulting fields with the Navy σ field in this region. Global fields were then produced by scaling the global σ field by the coefficient resulting from the linear regression. For the GLOBE dataset, the A/S and P-T-H fields can be calculated globally from the $30''$ dataset. However, the A/S field must again be scaled to be consistent with the values obtained where high-resolution data exist. The scaling factor is chosen so that the mean over the region where the $3''$ data exists is the same.

Clearly, neither of the above approaches is ideal. However, the global fields derived from the GLOBE dataset do at least include some of the scales relevant to the orographic roughness scheme (scales of the order of 5 km or less). In contrast, the Navy fields are derived from the global σ field, and thus are derived from a field that does not include any of the scales relevant to the orographic roughness scheme. We would, therefore, hope that the orographic roughness fields are more accurate when derived from the GLOBE dataset.

Except in the regions where high-resolution data are available, there are very large differences in these fields. The values derived from the GLOBE dataset are generally smaller than those derived from the Navy dataset. Over the Andes, in fact, the values of A/S derived from the GLOBE dataset are about half those derived from the Navy dataset. Thus, away from where there is high-resolution data, the amplitude of the response of the orographic roughness scheme will generally be reduced by moving to the GLOBE dataset.

3. Smoothing the orography

(*a*) *Motivation*

A fundamental limitation of any numerical model is that features close to the grid-scale are poorly resolved; at these scales truncation effects (numerical errors) will dominate the true solution. As emphasized by Lander and Hoskins (1997), it is therefore desirable that these scales should not be forced directly as otherwise the well-resolved scales may very soon be contaminated by the errors forced at, or close to, the grid-scale.

In spectral transform GCMs, grid-scale and near-grid-scale orography manifests itself as Gibbs oscillations in physical space. These spurious oscillations can cause problems for the physical parametrizations with, for example, elevated sea points resulting in spurious forcing of the large-scale and/or convective precipitation schemes. The reduction of these spurious oscillations, and hence the reduction in grid-scale and near-grid-scale orographic forcing, has therefore received significant attention in these GCMs (Navarra *et al.* 1994; Bouteloup 1995; Holzer 1996).

Smoothing the resolved orography in grid-point GCMs has received rather less attention. Indeed, at the Met Office, the operational numerical weather- and climate-prediction models have always used unfiltered mean orography. In recent years, however, this approach has led to problems associated with spurious forcing in the horizontal at the grid-scale. This forcing may result in localized, vertically coherent, vertical motions. In the old version of the UM, an increase in vertical resolution led to these vertical motions occasionally triggering a numerical instability when the Courant–Friedrichs–Lewy limit for vertical advection was violated over the Himalayas. In the new version of the UM, these vertical motions frequently triggered 'grid-point storms' (resolved convection at a single grid point), most notably over the mountains of Papua New Guinea. In both instances, the instabilities were extremely damaging to the model performance

and occasionally caused the model to 'blow up'. Thus, the case for smoothing the UM mean orography has become very obvious.

Recently, Davies and Brown (2001) investigated which scales of orography can be adequately resolved in a numerical model. Their work indicated that two-grid-length features cannot be adequately resolved, whilst six-grid-length features can be adequately resolved. At the four-grid-length scale, results were generally qualitatively accurate, but quantitatively inaccurate. This study has since been repeated using the dynamical core of the new version of the UM, and the results described above apply equally well to the new version of the model (L. Davies, personal communication).

The above study indicates that the filtering applied should eliminate two-grid-length features entirely whilst retaining six-grid-length (and above) features. The sixth-order implicit filter described in Raymond (1988), and hereafter referred to as the Raymond filter, is a suitable candidate as it eliminates two-grid-length features entirely and is scale selective via a parameter ϵ, with larger values of ϵ giving increased filtering. This parameter can therefore be adjusted to make the transition from filtering to no filtering consistent with the results of Davies and Brown (2001), and also to ensure that the instability problems highlighted above are inhibited.

(*b*) *Grid-scale and isotropic filtering of the mean orography*

The Raymond filter was developed for use within limited-area models. More precisely, the filter was developed for use in models with isotropic grids. In this section we describe the changes necessary to use the Raymond filter on an anisotropic grid on the sphere.

The Raymond filter has an amplitude response function of the form

$$F(\kappa) = \left\{1 + \epsilon \tan^6\left(\frac{\kappa r \Delta}{2}\right)\right\}^{-1}, \tag{1}$$

where κ is the wave number, r is the earth radius and Δ is the latitudinal or longitudinal grid resolution. In most of the experiments in section 6, ϵ is set equal to 1. This results in four-grid-length features being damped by half, whilst six-grid-length features are damped by less than 5% and so $\epsilon = 1$ is consistent with the results of Davies and Brown (2001). It was found that $\epsilon = 1$ was the smallest value that suppresses orographically triggered grid-point storms in the new version of the UM.

One issue to overcome when applying the Raymond filter to a spherical domain is how to implement the requirement for no filtering at the ends of the filtering domain. As a result of its implicit nature, the Raymond filter cannot be directly applied to the two points adjacent to the boundaries. At these points, in fact, the filter uses lower-order schemes whose errors propagate into the central domain. The cyclic nature of data in terms of latitude and longitude on the sphere allows us to simply repeat the points at one end of the filtering domain at the other end, thereby allowing the Raymond filter to be applied throughout. Four points were repeated at each end of the domain as this was found to be sufficient to reduce the boundary effects of the filter almost to zero.

A second issue to consider with regard to the spherical domain is the filtering of the mean orography so that the resolution is isotropic. If the orography is simply averaged over grid boxes then the filtering is not uniform, being strongly dependent on the location of the grid poles (which are not necessarily the same as the geographic poles). The regular latitude $\times$ longitude grid leads to increased east–west resolution in real space as the poles are approached. Thus, the mean orography should not simply be calculated as the grid-box average, but rather should be calculated as the mean over

a progressively greater longitudinal extent as the poles are approached. Ideally, this filtering should be done as part of the calculation of the mean orography from the source data. However, in the experiments described in this paper, the longitudinal averaging is actually done on the grid-box mean orography. Thus, the number of input data points M averaged together is given by

$$M = \max\{1, (\cos\phi)^{-1}\delta\phi/\delta\lambda\}, \tag{2}$$

where ϕ is the current latitude, $\delta\lambda$ is the longitudinal grid resolution and $\delta\phi$ the latitudinal grid resolution. Note that the average is as an arithmetic mean, with weights set according to the proportion of the input data point included in the average. Also, M is not necessarily an integer and so, for example, at a resolution of $0.83^\circ \times 1.25^\circ$ (as used in the forecast experiments in section 6), 68.8 points are averaged together at the latitude adjacent to the pole. In comparison to the grid-scale filtering, this isotropic filtering has only a small impact on the model simulation, and thus the exact method used is relatively unimportant.

Although the impact on the simulation of the isotropic filtering is small, its impact on the speed of convergence of the three-dimensional Helmholtz pressure solver used in the new version of the UM is rather more significant. Thus, since the experiments described in this paper were performed, the filtering implemented operationally has been changed. We believe the new implementation is more elegant and therefore describe it here for completeness. Essentially, the Raymond filter has been modified so that its filtering is isotropic on the sphere. Thus, the filtering scale in real space is the same at all latitudes as it is in the longitudinal direction. This is done by allowing ϵ to vary with latitude.

The filter is made isotropic by the following procedure. Since the grid resolution is constant in the meridional direction, only the filtering in the latitudinal direction need be modified. Let κ_ϕ be the wave number such that $F_\phi = 0.5$ for filtering in the meridional direction. Then ϵ_ϕ, the required filter strength, is given by

$$\epsilon_\phi = \tan^{-6}\left(\frac{\kappa_\phi r\delta\phi}{2}\right). \tag{3}$$

Then, in order that wave numbers κ_λ in the latitudinal direction, which are equal to κ_ϕ, have the same response (i.e. $F_\lambda = 0.5$), ϵ_λ is given by

$$\epsilon_\lambda(\phi) = \tan^{-6}\left(\frac{\kappa_\lambda r\cos\phi\delta\lambda}{2}\right). \tag{4}$$

However, this filtering is only applied polewards of where the grid is square and therefore

$$\epsilon_\lambda(\phi) = \tan^{-6}\left(\frac{\kappa_\lambda r\delta\phi}{2M}\right), \tag{5}$$

where M is as defined in Eq. (2). Thus, polewards of where the grid cells are square in reality, ϵ_λ exceeds ϵ_ϕ. Indeed, currently, $\epsilon_\phi = 1$ and so, for the forecast tests in section 6, the Raymond filter is required to damp the 275.2 (68.8×4) grid-length wave by 50%, and thus the value of ϵ_λ for the row adjacent to the South Pole is 9.27 billion!

Filtering the orography in the above manner, rather than in the manner applied in the experiments documented in this paper, leads to about a 2% reduction in the run time of the new version of the UM. However, as we have already said, the impact of this new filtering on the model simulation is very small, since the changes to the orography only

become significant polewards of about 80°. The new isotropic filtering may in the future be extended to the equator since currently Eq. (2) implies that the anisotropy of the grid is ignored in the Tropics. This has not yet been implemented operationally because the reduction in latitudinal filtering implied by this extension of the isotropic filter may require a reassessment of the smoothing required to ensure that grid-point storms do not reappear over orography, i.e. the length-scale of the filtering in real space (as set by ϵ_ϕ) may have to be increased.

(*c*) *The mismatch of the orography and the land–sea mask*

The filtering described above results in some small amplitude oscillations, most notably adjacent to the west side of the Andes. However, these oscillations die away very quickly, reducing in amplitude by about an order of magnitude from one trough to the next. Of greater concern is the impact of the filtering on steep slopes immediately adjacent to the sea. Whilst the smoothing reduces their steepness, it also results in these slopes extending over a greater horizontal distance, and this may result in sea points being elevated above sea level. At the horizontal resolution used in this paper, for example, a couple of sea points adjacent to the northern Andes are 1300 m above sea level. Clearly, displacing these points by this amount may cause very significant problems due to spurious forcing of the model parametrizations, and this should therefore be addressed in some way. Note that this problem must also occur in spectral transform GCMs, even when that orography has been smoothed to minimize Gibbs oscillations.

The approach adopted here to alleviate this problem is simply to set the elevation of all sea points (not including inland lakes or seas) to sea level. This obviously circumvents any problems associated with spuriously forced physics over sea points. The disadvantage of this approach is that grid-scale 'cliffs' are re-introduced into the orography field, most notably along the west side of the Andes. However, this approach was found to be as good as the alternative solution of adjusting the sea surface temperatures using some adiabatic lapse rate to account for their displacement from sea level. This alternative solution has been applied in several spectral transform GCMs (e.g. Navarra *et al.* 1994). In spectral transform GCMs, in fact, it is the only solution available because the global orography field must always be represented spectrally.

(*d*) *The filtering of the subgrid fields*

The final two issues concerning the specification of the UM orography are both associated with the SSO fields. The first issue is the calculation of the standard deviation field. This is now calculated relative to the filtered mean orography field rather than relative to the grid-box (unfiltered) mean. In this way, the information 'lost' from the mean orography by the filtering process is gained by the SSO field, and hence the scales that were previously poorly resolved are now parametrized by the SSO scheme. This approach has already been used by SM00.

The second issue is the filtering applied to the SSO fields. These fields have a less direct impact on the model evolution than the mean orography because they are just some of the inputs to the orography parametrizations. The other inputs are the low-level winds, stability and density of the large-scale flow. Although their impact is less direct, it is still clearly undesirable that grid-scale variations are present in these fields. Thus, these fields are filtered in exactly the same way as the mean orography. This includes the resetting of these fields to zero over the sea.

4. The new subgrid orographic drag scheme

(*a*) *Weaknesses of the 95 scheme*

The main features of the 95 scheme are as follows: For high Froude number ($F_r = U/Nh$, where U is a low-level wind speed, N a low-level buoyancy frequency, and h the subgrid mountain height) flows the scheme represents linear hydrostatic gravity waves and, for suitable tropospheric wind and stability profiles, trapped lee waves. For low F_r flows the scheme is based on the hydraulic jump response. The scheme is fully documented in GSM98. As illustrated by Milton and Wilson (1996), the 95 scheme had a large positive impact when it was implemented in the operational forecast model together with an orographic roughness scheme. However, although the scheme undoubtedly performed very well, a number of weaknesses have been identified. Here, we shall highlight a couple of these weaknesses.

Perhaps the most striking weakness of the 95 scheme is that it does not include an explicit representation of the drag associated with flow blocking at low F_r, i.e. the 95 scheme does not include a representation of the drag due to flow around SSO rather than flow over SSO. LM97 and SM00 have both shown significant improvements to global circulation model performance by incorporating the effects of flow blocking. In the 95 scheme, the low F_r response is based on the hydraulic jump regime, and this regime is typically invoked at half of all land points every time step. This is clearly excessive in comparison to the isolated instances of hydraulic jumps in reality (e.g. the Boulder downslope windstorm of 1972 (Lilly 1978)). However, it is also an inevitable consequence of this being the only response that can be invoked at low F_r. The hydraulic jump response usually results in a uniform drag being applied through much of the troposphere. The lack of an explicit flow-blocking parametrization is therefore likely to result in the parametrized drag being applied over too deep a layer.

A further weakness of the 95 scheme is associated with the definition of the wave-launching height h_l. This is defined as $h_l = \min(\sqrt{2}\sigma, 1000\ \text{m})$. The 1000 m limit was introduced to prevent the launching height reaching jet-stream levels over high terrain, most notably over the Himalayas. A more robust scheme would define h_l to be proportional to σ everywhere.

The new scheme described below addresses these and other weaknesses of the 95 scheme.

(*b*) *Rationale behind the new scheme*

The motivation for the new SSO scheme is provided by the modelling study of OB97 who performed a series of experiments of flow over an elliptical mountain. Figure 3 (adapted from their Fig. 4) summarizes the main result of their study. This figure shows the pressure drag for three of their experiments (non-rotating, rotating, and rotating with friction). The drag in all these experiments was normalized by that predicted analytically for linear two-dimensional non-rotating frictionless flow. The non-rotating runs exhibit the well-known variation in drag as F_r^{-1} is varied, with the high-drag hydraulic jump state evident when F_r^{-1} is of order unity, for example. These results, which were first documented in the 1980s (see e.g. Smith 1985), provided some of the motivation for the 95 scheme and for that of SM00.

The rationale for the new SSO scheme is drawn from the results of the numerical experiments for more realistic flow conditions, i.e. from the simulations that included both friction and rotation. In these runs the pressure drag is much less dependent on the low-level F_r, deviating by no more than about 30% from the normalizing value. Furthermore, OB97 also performed a smaller set of experiments using a circular, rather

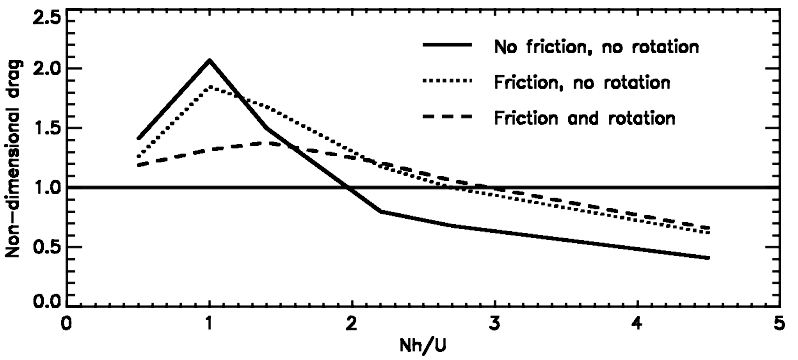

Figure 3. Simulated non-dimensional pressure drag on an elliptical mountain from Ólafsson and Bougeault (1997). The drag is normalized by the analytical expression for linear two-dimensional non-rotating frictionless flow.

than an elliptical, mountain. The results shown in Fig. 3 hold equally well for these simulations, i.e. the sensitivity of the drag to friction and rotation is independent of the shape of the mountain. OB97 suggested that their results with friction and rotation might help to explain why observed pressure drags, such as those measured in the PYREX experiment (Bessmoulin *et al.* 1993), agreed remarkably well with those predicted by the expression for linear two-dimensional non-rotating frictionless flow. The new scheme thus uses this simple normalizing value to predict the surface pressure drag, which is then within 30% of the correct value, irrespective of the incident flow's F_r and the SSO's precise shape. Note, however, that the shape of the subgrid orography does still influence the surface pressure drag because the relevant incident flow is still that perpendicular to the major axis of the SSO.

The surface pressure drag is then partitioned into a blocked-flow component and a GWD component depending on the F_r of the incident flow. This is done by defining a 'top layer' of the flow impinging on a mountain, whose depth is equal to the layer of air flowing over the mountain (following e.g. Hunt *et al.* (2001)). Equivalently, the depth of this layer is often referred to as the 'cut-off' mountain height or the 'summit region'. Consistent with the results of OB97, the gravity waves are assumed to be linear and hydrostatic. The gravity-wave amplitude is assumed to be proportional to the depth of the top layer and the remainder of the surface pressure drag is assumed to be due to flow blocking.

The new scheme is thus an empirical fit to the most realistic simulations of OB97 (i.e. those including both friction and rotation) and is conceptually similar to both LM97 and SM00, although simpler. In particular, the total surface pressure drag, which is partitioned into two components, is independent of the low-level F_r. The new scheme therefore provides a simple starting point from which to further develop the parametrization of the effects of SSO.

(*c*) *Description of the new scheme*

The total surface stress is given by the analytical expression for linear two-dimensional non-rotating frictionless flow. Following GSM98, the expression is modified to account for the anisotropy of the subgrid orography becoming

$$\tau_{sx} = \rho u N \widehat{K}^{-1}(\sigma_{xx} \cos\chi + \sigma_{xy} \sin\chi), \tag{6}$$

$$\tau_{sy} = \rho v N \widehat{K}^{-1}(\sigma_{xy} \cos\chi + \sigma_{yy} \sin\chi), \tag{7}$$

where τ_{sx} and τ_{sy} are the zonal and meridional components of the surface stress, respectively, ρ is the low-level density, u and v are the components of the low-level wind speed, χ is the direction of the low-level wind relative to westerly, $\widehat{K}$ is a 'tuneable' wave-number constant, and the σ_{ij} are the squared grid-box-average gradients of the source dataset as defined in section 2(b). Here, 'low-level' refers to the height of the subgrid mountains, h, and is set equal to 2.5σ which is slightly deeper than the generally accepted 2σ value for the tops of the subgrid mountains, e.g. Wallace *et al.* (1983). However, as we shall illustrate in section 6(a), the impact of this choice is actually very small.

The partitioning of the drag into blocked-flow and gravity-wave components is determined by the depth of the top layer t, which is diagnosed as

$$t = \frac{U}{F_{rc} N}, \tag{8}$$

where U is the component of the wind $\mathbf{U} = (u, v)$ in the direction of the surface stress vector $\boldsymbol{\tau}_s = (\tau_{sx}, \tau_{sy})$ and F_{rc} is the F_r at which flow blocking is deemed to first occur. This should be of order unity but, equally, it is legitimate to treat F_{rc} as a tuneable parameter. One reason for taking this approach is that the U and N used in Eq. (8) are averages over the full height of the subgrid mountains. The effect of the shear of the incident flow, which may influence the depth of the top layer, is therefore neglected.

Once the depth of the top layer is known, the gravity-wave component of the surface stress can be evaluated as

$$\boldsymbol{\tau}_{gwd} = \boldsymbol{\tau}_s \cdot \left(\frac{t}{h}\right)^2. \tag{9}$$

The amplitude of the waves is thus proportional to the depth of the top layer rather than the full depth of the subgrid mountains. Note that these depths are equal when $F_r \geq F_{rc}$. The remainder of the surface stress, $\boldsymbol{\tau}_{bf}$ is attributed to flow blocking, i.e.

$$\boldsymbol{\tau}_{bf} = \boldsymbol{\tau}_s - \boldsymbol{\tau}_{gwd}. \tag{10}$$

Thus, $\boldsymbol{\tau}_{bf}$ is simply the consequence of our empirical fit to the results of OB97.

The diagnosis of gravity-wave breaking, and hence the deposition of $\boldsymbol{\tau}_{gwd}$ in the vertical, uses the same saturation hypothesis as GSM98, with the waves launched from height h. The vertical deposition of $\boldsymbol{\tau}_{bf}$ is simply assumed to be uniform throughout the depth h of the whole layer, rather than just the depth of the blocked layer ($d = h - t$). There is very little difference in the results but certain numerical problems are obviated. These could occur because the $\mathbf{U}$ used to calculate $\boldsymbol{\tau}_s$ is an average over h. If no drag is applied in layer t then it would be possible for the average U to remain unchanged even though the wind in the blocked layer continued to be slowed. This process could thus reverse the winds in the blocked layer relative to those in layer t. With the approach taken here, the total surface stress reduces from $\boldsymbol{\tau}_s$ at the ground to $\boldsymbol{\tau}_{gwd}$ at height h. Above this level, the stress remains constant with height unless wave breaking is diagnosed.

In summary, the new scheme is very simple, both in the way the surface stress is diagnosed and in the way in which this stress is deposited in the vertical. The scheme has only two free parameters, namely $\widehat{K}^{-1}$, which determines the amplitude of the parametrized response, and F_{rc}, which determines the partitioning of the drag into gravity-wave and blocked-flow components. These features make the scheme simple to implement numerically and simple to understand. As we shall see in section 6(a), this in turn makes the optimal tuning of the free parameters a relatively simple process.

In comparison to the schemes of SM00 and LM97, the main differences appear to occur at low F_r. In this regime the total surface pressure drag will be significantly larger than in SM00 and comparable to that in LM97 (see SM00 for an evaluation of the normalized pressure drag for these two schemes). An important difference to LM97 is that the new scheme applies much more drag in the blocked layer at low F_r. In LM97, most of the drag at low F_r is actually attributed to gravity waves rather than to blocked flow. Thus most of the drag in the LM97 scheme is applied above the blocked layer rather than in it. LM97 comment that their gravity-wave surface stress is overly large at low F_r because it is proportional to the square of the full subgrid mountain height h rather than to the square of the top-layer depth t. They argue that this should not be that important at low F_r since this regime often corresponds to weak winds and hence to a small drag. However, if $F_r = 0.1$, for example, the LM97 scheme would overpredict the gravity-wave surface stress by two orders of magnitude. Over the Himalayas, h may exceed 2000 m and so the winds need not be that weak to give a low F_r. Thus, the discrepancy could actually have a large impact on the predicted drag.

5. The new version of the Unified Model

The new version of the UM is very different from the old version (Cullen 1993), with a new dynamical core and significant improvements to many physical parametrizations. A brief outline of these changes is given below. A more detailed description of many of these changes can be found in Cullen *et al.* (1997) and Davies *et al.* (1999).

The main changes to the dynamical core of the new version of the UM are as follows. The hydrostatic assumption is no longer made so the underlying equations are the fully compressible, non-hydrostatic, deep-atmosphere equations (see Thuburn *et al.* (2002) for discussion of the unforced equation set). These equations are discretized using a predictor-corrector approach to a two-time-level semi-implicit semi-Lagrangian scheme. The grid staggering in the horizontal is the Arakawa 'C' grid, whilst in the vertical a Charney–Phillips staggering is employed. The vertical coordinate is height based, with terrain following levels at the ground smoothly transitioning to 'flat' levels (concentric spheres) aloft.

The inclusion of non-hydrostatic effects together with the use of a two-time-level scheme imply that the semi-implicit scheme requires the solution of a variable coefficient problem. The Helmholtz equation which results is solved using a generalized conjugate residual method described in Smolarkiewicz and Margolin (1994). On the sphere, preconditioning in both the horizontal and the vertical are required to achieve convergence within a tolerable number of iterations. The preconditioning in the horizontal is required to compensate for the increased east–west resolution at high latitudes due to the convergence of the meridians of the regular latitude $\times$ longitude grid. An alternating direction implicit preconditioning technique, as proposed by Skamarock *et al.* (1996), is thus applied longitudinally and vertically.

As we have already mentioned, most of the physical parametrizations have been significantly upgraded in the new model. The basic radiation scheme is described in Edwards and Slingo (1996), with the treatment of gaseous absorption following Cusack *et al.* (1999) and the treatment of ice crystals following Kristjansson *et al.* (2000). The boundary-layer scheme is that described by Lock *et al.* (2000) and includes non-local mixing in unstable regimes. The scheme also includes the revisions to entrainment in convective regimes described by Lock (2001). The convection scheme is based on that described in Gregory and Rowntree (1990). However, significant changes have been made. The diagnosis of shallow and deep convection is based on the diagnosed

boundary-layer type. The cloud base is defined as the lifting condensation level. The thermodynamic cloud-base closure for shallow convection follows Grant (2001) and for deep convection is based on the reduction to zero of convectively available potential energy over a given time-scale (following Fritsch and Chappell (1980)). Convective momentum transports are based on a flux-gradient relationship with the cloud-base closure based on the assumption that large-scale horizontal pressure gradients should be continuous across the cloud base. Entrainment and detrainment rates for shallow convection are based on the results of Grant and Brown (1999). Land-surface processes are incorporated using the Met Office surface exchange scheme (Cox *et al.* 1999). The representation of large-scale cloud and precipitation includes a prognostic treatment of ice microphysics (Wilson and Ballard 1999).

In the forecast tests described in section 6, the model is run with a latitude $\times$ longitude resolution of $0.83^\circ \times 1.25^\circ$. Thirty-eight levels are used in the vertical, concentrating 12 levels in the lowest 2 km to give higher resolution near the ground. The model lid is placed at about 39 km. A time step of 20 min is employed, except for the convection scheme which uses a time step of 10 min, since otherwise the convective mass fluxes could be numerically limited.

6. Results

In this section we shall illustrate the impact of the new orography package (hereafter the NEW package) in the new version of the UM. The results are documented in three subsections. In section 6(a), we try to separate out the impact of the new SSO scheme from the other two components of the NEW package. Additionally, a series of experiments is performed to illustrate the sensitivity of the new SSO scheme to the values of its free parameters. Sections 6(b) and (c) focus on a one-month forecast trial, which includes full data assimilation, that has been run with the NEW package. Section 6(b) illustrates the changes in the modelled orography response, whilst section 6(c) describes the impact of the NEW package on the forecast skill of the new version of the UM.

(*a*) *Sensitivity experiments with the NEW package*

A total of ten different experiments, each consisting of five individual forecasts, have been run to illustrate the sensitivity of the NEW package. The first set has been run to isolate the impact of the new SSO scheme from the impact of the GLOBE dataset and the smoothing, while the second set illustrates the sensitivity of the NEW package to the values of the free parameters in the new SSO scheme. Each forecast is for five days (T+120) and is initialized with the 1200 UTC Met Office operational analysis interpolated to the new UM grid. The analysis dates for the five forecasts are 1 December 1999, 15 December 1999, 15 January 2000, 3 February 2000 and 15 February 2000. Validation of each forecast was performed relative to the operational analysis for that time.

It is important to note that we cannot be completely confident of the statistical significance of these tests since there will be considerable natural variability left unsampled when only five separate forecasts are performed. The amplitude and even the sign of the impact of a particular change on forecast performance may therefore be in error. However, we are confident that the size of the impact of one change relative to another is robust, since a large impact in one field (e.g. northern hemisphere mean-sea-level pressure) has been found to be accompanied by similarly large changes in other fields (e.g. tropical 850 hPa winds).

TABLE 1. CONFIGURATION OF THE FORECAST SENSITIVITY EXPERIMENTS

Experiment	Dataset	Smoothing (ϵ)	SSO scheme	$\widehat{K}^{-1}$	F_{rc}	h/σ
OLD	Navy	0.1	old	1×10^4	n/a	n/a
NEW	GLOBE	1	new	1×10^5	2	2.5
NEWnavy	Navy	1	new	5×10^4	2	2.5
NEWeps01	GLOBE	0.1	new	1×10^5	2	2.5
NEWunfilt	GLOBE	unfiltered	new	1×10^5	2	2.5
OLDglobe	GLOBE	0.1	old	2×10^4	n/a	n/a
NEWk−	GLOBE	1	new	5×10^4	2	2.5
NEWk+	GLOBE	1	new	1.5×10^5	2	2.5
NEWfrc1	GLOBE	1	new	1×10^5	1	2.5
NEW2sig	GLOBE	1	new	1×10^5	2	2

See text for definition of symbols.

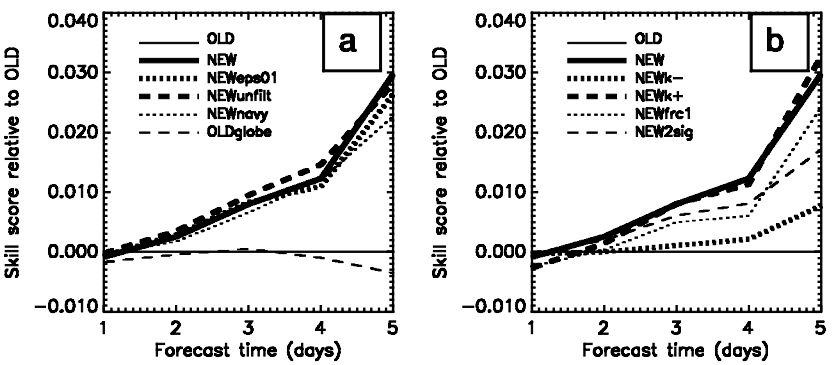

Figure 4. Northern hemisphere (north of 20°N) mean-sea-level pressure skill score for the experiments listed in Table 1, relative to the skill of experiment OLD. The skill score is the root-mean-square (r.m.s.) error normalized by the persistence r.m.s. error, and the verification is relative to operational forecast analyses.

The various experiments are listed in Table 1. Note that the OLD package uses the Navy dataset, the old SSO scheme and a Raymond-filtered orography with $\epsilon = 0.1$. Some filtering is applied in this package because, as mentioned in section 3(a), the new version of the UM regularly suffers from grid-point storms over orography when this filtering is not applied. This additional filtering is the only difference between the OLD package and that of the old version of the UM.

Figure 4 shows the northern hemisphere (>20°N, hereafter NH) mean-sea-level pressure (MSLP) forecast skill for the experiments listed in Table 1 relative to the OLD package. Here, forecast skill is defined as the root-mean-square (r.m.s.) error normalized by the persistence r.m.s. error. Unless otherwise stated, the conclusions drawn from this plot are consistent with those for all other fields verified in the NH, the Tropics (equatorwards of 20°) and the southern hemisphere (>20°S, hereafter SH). The other fields verified, namely MSLP, 500 hPa height and 250 hPa winds in the NH and SH, and 850 and 250 hPa winds in the Tropics, are those routinely verified at the Met Office.

Figure 4(a) shows the MSLP skill scores from the series of experiments that attempt to isolate the impact of the three different components in the NEW package. It is apparent that almost all the difference between the NEW and OLD packages is due to the change in SSO scheme. Both the impact of the GLOBE dataset, as seen by comparing the NEW package with NEWnavy and the OLD package with OLDglobe, and the impact of the smoothing, as seen in by comparing the NEW package with NEWeps01

and NEWunfilt, are small. Note that the value of $\widehat{K}^{-1}$ in experiments NEWnavy and OLDglobe was adjusted to compensate for the σ_{xx}, σ_{xy} and σ_{yy} differences between the two datasets.

Figure 4(b) shows the various experiments performed to illustrate the sensitivity of the new SSO scheme. Comparing experiments NEWk+ and NEWk− with the NEW package shows that the new SSO scheme has only a small sensitivity to $\widehat{K}^{-1}$ (as long as it is not too small, i.e. except experiment NEWk−). Similarly, comparing experiments NEWfrc1 and NEW2sig to the NEW package shows that the new SSO scheme has only a small sensitivity to F_{rc} and to h. This somewhat surprising lack of sensitivity is primarily due to the negative feedback of the low-level drag on the surface stress which is large because most of the surface stress is usually attributed to low-level flow blocking. This drag is applied uniformly over the full height of the subgrid mountains, h, which is the same layer over which the winds are averaged for the calculation of the surface stress. Thus, for a larger (smaller) value of $\widehat{K}^{-1}$, a larger (smaller) drag will be applied over the layer h. At the next time step, the reduced (increased) winds in this layer will reduce (increase) the surface stress and reduce (increased) the drag being applied in this layer. In this way the new SSO scheme may reach a similar equilibrium state for a range of parameter settings.

One point not evident from Fig. 4(b) is the inferior performance of experiment NEWfrc1. This was very striking in the NH at the 250 hPa level, where the wind errors in this experiment were much bigger than in any of the other nine experiments. The reduction in F_{rc} increased the surface stress attributed to gravity waves and this resulted in very large drags being exerted in the lower stratosphere, most notably over the Himalayas. Even by day 1 this drag had, via geostrophic adjustment, reduced the winds below at the 250 hPa level, which led to a large reduction in forecast skill at this level.

In summary, these sensitivity experiments have shown that the impact of the NEW package is dominated by the new SSO scheme. The impact of the new SSO scheme is, within the range of parameters explored, relatively insensitive to its free parameters. The NEW package therefore appears to be reasonably close to the optimum configuration. In the next two subsections the NEW package is compared with the OLD package in a one month forecast trial including data assimilation.

(*b*) *Impact on the modelled orography response*

The NEW package has been more rigorously compared with the OLD package by performing a pair of one-month (December 1999) forecast trials that include the three-dimensional variational data assimilation scheme of Lorenc *et al.* (2000). Each trial thus has an independent assimilation cycle with trial forecasts being run each day, starting from a 1200 UTC analysis, for five days ahead.

In this subsection the differences between the modelled orography responses in the two trials are discussed. The fields shown are averages of the 31 forecasts in each trial. The important changes in the modelled orography response are illustrated in Fig. 5, which shows the zonal-mean magnitude of the boundary layer (BL) and SSO surface stresses. Note that the resolved stresses are not shown because the differences are very small, even though local differences are significant, consistent with the mean orography differences shown in Fig. 2. Figure 5(a) shows that the BL stresses are generally slightly reduced with the NEW package, particularly away from the northern midlatitudes, where high-resolution data were available to create the A/S and P-T-H fields. An inspection of the BL stresses in the sensitivity experiments of the previous

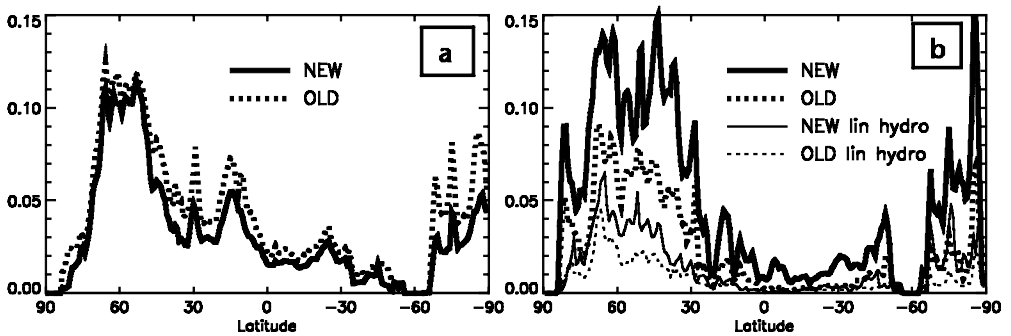

Figure 5. The zonal-mean magnitude of the surface stresses for (a) the boundary-layer scheme (for land points only) and (b) the SSO scheme. The stresses for the NEW and OLD packages are shown with solid and dotted lines, respectively. In (b) the total stresses are shown with thick solid lines whilst the linear hydrostatic gravity-wave stresses are shown with thin lines. The units of stress are N m^{-2}.

section (not shown) indicates that this change is indeed dominated by the change in the A/S and P-T-H fields caused by the change in dataset. The change in BL stresses due to the change in SSO scheme is rather smaller by comparison.

Figure 5(b) shows the zonal-mean magnitude of the SSO surface stress for the two trials. The largest difference is seen in the total SSO stress which is approximately doubled with the NEW package in the NH. An inspection of the geographical distribution of these stresses (not shown) indicates that this large zonal-mean difference is primarily due to the NEW package producing significant stresses where the OLD package produced almost none, e.g. over the western side of the Tibetan Plateau. This signal is also seen in the Tropics and SH and, indeed, is evident in Fig. 5(b) between the equator and 30°S, which is a result of large changes in stress over the northern Andes. In regions where the OLD package produces large stresses the NEW package tends to produce stresses of comparable magnitude.

Interestingly, and perhaps somewhat surprisingly, the large change in the magnitude of the surface stress in the two trials has only a small impact on the zonal-mean torque (where torque $= \tau_{sx} r \cos(\phi)$). In general, the zonal-mean SSO torque changes by only about 25% as opposed to the 100% change noted above for the stress magnitude. Furthermore, most of the increase in the zonal-mean SSO torque is offset by a decrease in the zonal-mean BL torque. Thus, the overall impact of the NEW package is rather smaller than might first have been thought from Fig. 5. Indeed, the small difference in the total zonal-mean torque in the two trials is probably no coincidence and merely reflects the implicit tuning of both SSO schemes to minimize forecast errors.

The thin lines in Fig. 5(b) show the zonal-mean magnitude of the linear hydrostatic gravity-wave stresses for the two SSO schemes. These stresses are generally slightly greater with the NEW package, particularly over the latitude belt from 40°N–70°N. In general, about 20–30% of the total surface stress is due to linear hydrostatic gravity waves in the NEW package, i.e. most of the total surface stress is attributed to flow blocking. For the OLD package, of the order of 40% of the total surface stress is attributed to linear hydrostatic gravity waves and about 60% is attributed to hydraulic jumps and trapped lee waves.

Figure 6 shows the zonal-mean acceleration of the zonal wind due to the two SSO schemes. The most striking feature is the increase in drag at low levels with the NEW package, which is consistent with the introduction of the low-level flow-blocking scheme. Significant low-level drags that are not present with the OLD package are also

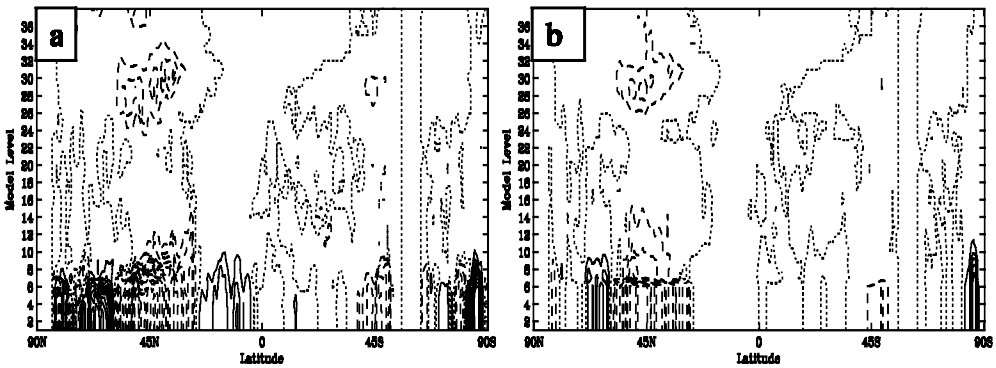

Figure 6. The average T+24 (1 day) SSO zonal-mean zonal wind acceleration for (a) the NEW package and (b) the OLD package. The model levels are numbered sequentially beginning with the level nearest the ground. Solid lines denote positive values, dashed lines denote negative values whilst the dotted line denotes the zero contour. The contour interval is 0.5 m $s^{-1}d^{-1}$.

evident in the Tropics and SH. As we shall see in the next subsection, the extra low-level drag in both the NH and in the Tropics improves the forecast skill of the NEW package.

The increased linear hydrostatic gravity-wave stresses evident from 40°N–70°N in Fig. 5(b) lead to an increased drag in the lower stratosphere (around model level 30). An inspection of latitude × longitude sections at these levels indicates that the increased drag is mainly over the Rockies (not shown). The increase in linear hydrostatic gravity-wave stresses in the NEW package actually makes the upper-level simulation worse. This suggests that an increase in F_{rc}, and hence a reduction in the proportion of the surface stress attributed to gravity waves, could further improve the forecast performance of the NEW package.

One final point to note in Fig. 6(b) is the level dependency of the OLD package, with most of the low-level drag confined below model level 7, which is the model level closest to the wave launching height h_1. Over the major mountain ranges, where most of the parametrized drag is applied, the 1000 m limit dominates. Much of the drag below model level 7 is actually due to trapped lee waves as a result of the way in which trapped lee waves are diagnosed, which involves finding the optimum height of an interface between two layers of equal depth. The optimum height for this interface is often diagnosed to be very close to the ground, but is constrained to be at least h_1 above the ground. Thus, since most of the lee-wave drag is applied in the lower of the two layers of equal depth, this diagnosis leads to most of the lee-wave drag being applied uniformly from the ground up to h_1. Much of the low-level drag in the 95 scheme is therefore due to a spurious diagnosis of trapped lee waves. No such level dependency is evident with the NEW package (Fig. 6(a)).

(*c*) *Impact on forecast skill*

The forecast skill of the two trials has been assessed by verifying the same fields as those in section 6(a) against surface and radiosonde observations and also against each trial's own analyses. Note that differences in r.m.s. errors of 2% or more are statistically significant for this length of forecast trial.

The NEW package leads to a number of statistically significant improvements in forecast skill, most notably in the NH in both MSLP and 500 hPa height fields. The largest improvements are seen in the T+24 r.m.s. MSLP errors, which improve by 3.4%

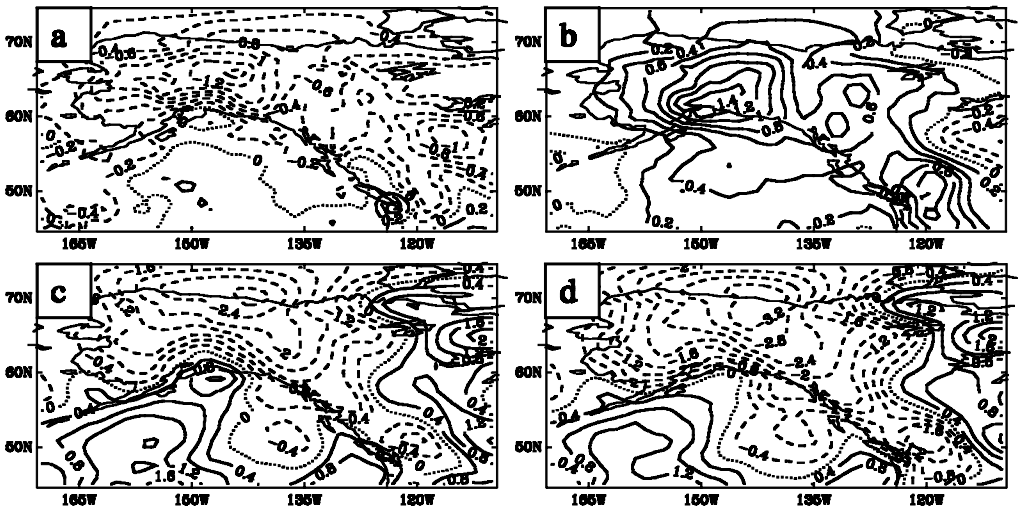

Figure 7. The average T+24 mean-sea-level pressure (MSLP) errors over north-west North America. (a) The difference in r.m.s. MSLP error between the two trials (NEW−OLD). (b) The difference in mean MSLP error between the two trials. (c) The mean MSLP error in the NEW trial. (d) The mean MSLP error in the OLD trial. The contour interval in (a) and (b) is 0.2 hPa, whilst in (c) and (d) the contour interval is 0.4 hPa. Solid lines denote positive values, dashed lines denote negative values whilst the dotted line denotes the zero contour.

when verified against observations and by 4.6% when verified against analyses. Low-level tropical winds are also significantly improved, most notably when verified against observations. The impact on all other fields was not significant. Thus, overall, the NEW package improves the forecast skill of the new version of the UM.

The reason behind the largest improvement in forecast skill, i.e. the reduction in T+24 NH r.m.s. MSLP error, has been investigated in more detail. This improvement occurs in the hemisphere and season in which the impact of orography is largest and, since it occurs early in the forecast at T+24, when the response is most linear. The largest reduction in r.m.s. MSLP error is over the northern Rockies and Alaska (Figure 7(a)). The largest (absolute) reductions of about 1.4 hPa equate to a 35% relative reduction in r.m.s. error at these locations. Figure 7(b) shows the change in mean MSLP error for the same region and is thus the difference between Figs. 7(c) and (d), which show the mean errors of the two trials in this region. It would appear from these plots that a large part of the reduction in r.m.s. error is, in part at least, due to a reduction in mean error. The interesting feature in Fig. 7(b) is that the reduction in mean error is due to a more anticyclonic circulation over Alaska.

Figure 8 shows the low-level SSO drag in this region for the two trials. Consistent with Fig. 6(a), more drag is applied at low levels with the NEW package. However, the important feature to note is the big increase in the low-level drag along the eastern flank of the mean MSLP error in Fig. 7(b). This increase in drag acts to reduce the poleward flow in this region, and hence is consistent with the anticyclonic circulation in Fig. 7(b). The largest improvement in forecast skill with the NEW package therefore appears to be due to the increased low-level drag over the mountains of south-eastern Alaska. The increased low-level drag is a result of the introduction of the flow-blocking scheme.

An extended forecast trial has also been performed for the NH summer season, although a detailed analysis of the impact of the NEW package in this trial has not been performed. However, overall, the impact of the NEW package in this trial was broadly

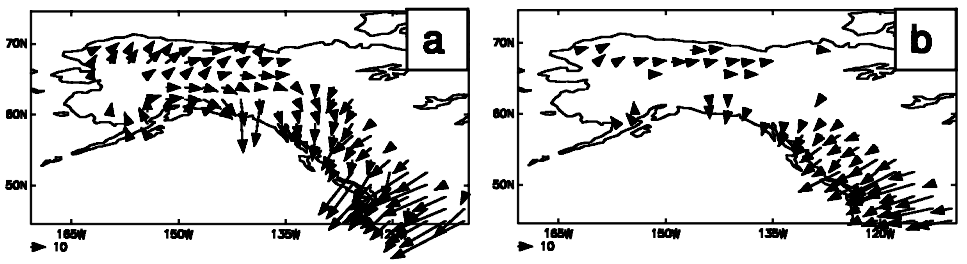

Figure 8. The T+24 layer averaged low-level deceleration of the large-scale flow: (a) in the NEW trial and (b) in the OLD trial. The averaging is mass weighted and performed over the lowest 13 model levels which equates to the lowest 2.5 km of the atmosphere. The units are m $s^{-1}d^{-1}$, with the size of the deceleration being proportional to the arrow length, and the arrow length being normalized by the 10 m $s^{-1}d^{-1}$ arrow shown below each panel. For clarity, only every second arrow is shown and then only if the amplitude exceeds 5 m $s^{-1}d^{-1}$.

neutral. Thus, on the basis of these two extended forecast trials, the NEW package has been incorporated into the new version of the UM.

7. Concluding remarks

In this paper we have presented three separate improvements to the representation of orography in a global numerical weather-prediction model (NWPM). The first of these is to use a new source dataset to calculate the orography fields input to the NWPM, thereby improving the fidelity of the representation of the earth topography in the NWPM. The second is to apply a scale-selective filter to the fields used by the NWPM to remove near-grid-scale features. This filtering improves the treatment of orography by ensuring that the NWPM is only forced at those scales it can represent well. The third improvement is to implement a new parametrization of the drag due to subgrid-scale orography. Taken together as a single package, the three improvements significantly enhance the forecast performance of the new version of the Met Office Unified Model (UM) in a northern hemisphere wintertime trial. A series of sensitivity experiments showed that the new SSO scheme is the dominant factor in this package. The enhanced forecast performance thus reflects the improved representation of SSO of the new scheme. The new package has therefore been incorporated into the new version of the UM and used in operational forecast runs since 7 August 2002.

An interesting issue to have been illustrated in this paper is the large sensitivity that the higher-order properties of the SSO, such as those that describe the anisotropy, may have to the source dataset. The sensitivity to the source data is part of the more general problem associated with the higher-order properties of the SSO pointed out by Taylor *et al.* (1997). They showed that the higher-order properties of the SSO converge much more slowly than lower-order properties (e.g. the standard deviation) as the resolution of the source dataset increases. This lack of robustness in the description of the SSO clearly needs addressing in some way. In this paper this was addressed by simply retuning the SSO scheme to produce similar drags with either dataset. As mentioned in section 2, an alternative to make the higher-order properties more robust would be to filter the source data to remove the smallest scales which are deemed not to be appropriate to the SSO scheme. Ultimately, however, the most robust solution will be to modify the method of describing the anisotropy of the SSO so that it depends on properties which converge more quickly. Defining this method will be the subject of future research at the Met Office.

Finally, the simplicity of the new SSO scheme has allowed us to implement it in a numerically robust way, i.e. its behaviour is independent of vertical resolution and the absence of any abrupt regime changes ensures that it is temporally smooth. The smoothing applied in the horizontal to the fields used by the SSO scheme ensures that the scheme does not produce forcing at the horizontal grid-scale. This robustness is borne out by the fact that the new package is now being used in the new version of the UM with the same values of $\widehat{K}^{-1}$ and F_{rc} for a wide range of horizontal resolutions, from the $2.5^\circ \times 3.75^\circ$ resolution used in extended climate simulations through to the $0.55^\circ \times 0.83^\circ$ used in the operational forecast model. The new package therefore provides a sound framework for future developments in the representation of orography in the UM.

Acknowledgements

We would like to thank many colleagues at the Met Office for many useful discussions during the course of this work and for their helpful comments on an earlier draft of this paper. We would also like to thank Ian Culverwell, Glenn Greed and Ding Min Li for running the extended forecast trials described in sections 6(b) and (c). Aidan McDonald kindly provided us with the computer code for the Raymond filter.

References

Bessmoulin, P., Bougeault, P., Genoves, A., Clar, A. J. and Puech, D. 1993 Mountain pressure drag during PYREX. *Beitr. Phys. Atmos*, **66,** 305–325

Bouteloup, Y. 1995 Improvement of the spectral representation of the Earth topography with a variational method. *Mon. Weather Rev.*, **123,** 1560–1573

Cox, P. M., Betts, R. A., Bunton, C. D., Essery, R. L. H., Rowntree, P. R. and Smith, J. 1999 The impact of new land surface physics on the GCM simulation of climate and climate sensitivity. *Clim. Dyn.*, **15,** 183–203

Cullen, M. J. P. 1993 The unified forecast/climate model. *Meteorol. Mag.*, **122,** 81–94

Cullen, M. J. P., Davies, T., Mawson, M. H., James, J. A. and Coulter, S. 1997 'An overview of numerical methods for the next generation of NWP and climate models'. Pp. 425–444 in *Numerical methods in atmosphere and ocean modelling. The Andre Robert memorial volume.* Eds. C. Lin, R. Laprise and H. Ritchie. Canadian Meteorological and Oceanographic Society, Ottawa, Canada

Cusack, S., Edwards, J. M. and Crowther, J. M. 1999 Investigating k distribution methods for parameterizing gaseous absorption in the Hadley Centre Climate Model. *J. Geophys. Res.*, **104,** 2051–2057

Davies, L. A. and Brown, A. R. 2001 Assessment of which scales of orography can be credibly resolved in a numerical model. *Q. J. R. Meteorol. Soc.*, **127,** 1225–1237

Davies, T., Cullen, M. J. P., Mawson, M. H. and Malcolm, A. J. 1999 'A New Dynamical formulation for the UK Meteorological Office Unified Model'. Pp. 202–225 in Proceedings of ECMWF seminar on recent developments in numerical methods for atmospheric modelling, 7–11 September 1998. European Centre for Medium-Range Weather Forecasts, Shinfield Park, Reading, Berkshire RG2 9AX, UK

Edwards, J. M. and Slingo, A. 1996 Studies with a flexible new radiation code. Part I: Choosing a configuration for a large-scale model. *Q. J. R. Meteorol. Soc.*, **122,** 689–719

Fritsch, J. M. and Chappell, C. F. 1980 Numerical prediction of convectively driven mesoscale pressure systems. Part I: Convective parameterization. *J. Atmos. Sci.*, **37,** 1722–1733

GLOBE Task Team	1999	The Global Land One-kilometer Base Elevation (GLOBE) Digital Elevation Model, Version 1.0. Eds. D. A. Hastings, P. K. Dunbar, G. M. Elphingstone, M. Bootz, H. Murakami, H. Maruyama, H. Masaharu, P. Holland, J. Payne, N. A. Bryant, T. L. Logan, J.-P. Muller, G. Schreier and J. S. MacDonald. National Oceanic and Atmospheric Administration, National Geophysical Data Center, 325 Broadway, Boulder, Colorado 80303, USA. Digital data base on the World Wide Web (URL: http://www.ngdc.noaa.gov/seg/to po/globe.shtml) and CD-ROMs.
Grant, A. L. M.	2001	Cloud-base fluxes in the cumulus-capped boundary layer. *Q. J. R. Meteorol. Soc.*, **127,** 407–421
Grant, A. L. M. and Brown, A. R.	1999	A similarity hypothesis for shallow-cumulus transports. *Q. J. R. Meteorol. Soc.*, **125,** 1913–1936
Gregory, D. and Rowntree, P. R.	1990	A mass flux scheme with representation of cloud ensemble characteristics and stability dependent closure. *Mon. Weather Rev.*, **118,** 1483–1506
Gregory, D., Shutts, G. J. and Mitchell, J. R.	1998	A new gravity-wave-drag scheme incorporating anisotropic orography and low-level wave breaking: Impact upon the climate of the UK Meteorological Office Unified Model. *Q. J. R. Meteorol. Soc.*, **124,** 463–493
Holzer, M.	1996	Optimal spectral topography and its effect on model climate. *J. Climate*, **9,** 2443–2463
Hunt, J. C. R., Ólafsson, H. and Bougeault, P.	2001	Coriolis effects on orographic and mesoscale flows. *Q. J. R. Meteorol. Soc.*, **127,** 601–633
Kristjansson, J. E., Edwards, J. M. and Mitchell, D. L.	2000	Impact of a new scheme for the optical properties of ice crystals on the climates of two GCMs. *J. Geophys. Res.*, **105,** 10063–10079
Lander, J. and Hoskins, B. J.	1997	Believable scales and parameterizations in a spectral transform model. *Mon. Weather Rev.*, **125,** 292–303
Lilly, D. K.	1978	A severe downslope windstorm and aircraft turbulence event induced by a mountain wave. *J. Atmos. Sci.*, **35,** 59–77
Lock, A. P.	2001	The numerical representation of entrainment in parameterizations of boundary layer turbulent mixing. *Mon. Weather Rev.*, **129,** 1148–1163
Lock, A. P., Brown, A. R., Bush, M. R., Martin, G. M. and Smith, R. N. B.	2000	A new boundary layer mixing scheme. Part I. Scheme description and single-column model tests. *Mon. Weather Rev.*, **128,** 3189–3199
Lorenc, A. C., Ballard, S. P., Bell, R. S., Ingleby, N. B., Andrews, P. L. F., Barker, D. M., Bray, J. R., Clayton, A. M., Dalby, T. D., Li, D., Payne, T. J. and Saunders, F. W.	2000	The Met. Office global three-dimensional variational data assimilation scheme. *Q. J. R. Meteorol. Soc.*, **126,** 2991–3012
Lott, F. and Miller, M. J.	1997	A new subgrid-scale orographic drag parametrization: Its formulation and testing. *Q. J. R. Meteorol. Soc.*, **123,** 101–127
McFarlane, N. A.	1987	The effect of orographically excited gravity wave drag on the circulation of the lower stratosphere and troposphere. *J. Atmos. Sci.*, **44,** 1775–1800
Mason, P. J.	1985	'On the parametrization of orographic drag'. Pp. 139–165 in proceedings of ECMWF seminar, on physical parametrization of numerical models of the atmosphere, 9–13 September 1985. European Centre for Medium-Range Weather Forecasts, Shinfield Park, Reading, Berkshire RG2 9AX, UK
Milton, S. F. and Wilson, C. A.	1996	The impact of parameterized subgrid-scale orographic forcing on systematic errors in a global NWP model. *Mon. Weather Rev.*, **124,** 2023–2045
Navarra, A., Stern, W. F. and Miyakoda, K.	1994	Reduction of the Gibbs oscillation in spectral model simulations. *J. Climate*, **7,** 1169–1183
Ólafsson, H. and Bougeault, P.	1997	The effect of rotation and surface friction on orographic drag. *J. Atmos. Sci.*, **54,** 193–210
Palmer, T. N., Shutts, G. J. and Swinbank, R.	1986	Alleviation of a systematic westerly bias in general-circulation and numerical weather-prediction models through an orographic gravity-wave drag parametrization. *Q. J. R. Meteorol. Soc.*, **112,** 1001–1039

Raymond, W. H. 1988 High-order low-pass implicit tangent filters for use in finite area calculations. *Mon. Weather Rev.*, **116,** 2132–2141

Scinocca, J. F. and McFarlane, N. A. 2000 The parametrization of drag induced by stratified flow over anisotropic orography. *Q. J. R. Meteorol. Soc.*, **126,** 2353–2393

Skamarock, W. C., Smolarkiewicz, P. K. and Klemp, J. B. 1996 Preconditioned conjugate-residual solvers for Helmholtz equations in non-hydrostatic models. *Mon. Weather Rev.*, **125,** 587–599

Smith, R. B. 1985 On severe downslope winds. *J. Atmos. Sci.*, **42,** 2597–2603

Smolarkiewicz, P. K. and Margolin, L. G. 1994 Variational Solver for elliptic problems in atmospheric flows. *Appl. Math. and Comp. Sci.*, **4,** 527–551

Taylor, P. A., Gong, W., Mengesha, Y., Weng, W., Xu, D. and Zhou, J. 1997 'Boundary-layer modelling of neutral and stably-stratified flow over hills, with emphasis on the drag'. Pp. 1–21 in proceedings of ECMWF seminar on orography, 10–12 November 1997. European Centre for Medium-Range Weather Forecasts, Shinfield Park, Reading, Berkshire RG2 9AX, UK

Thuburn, J., Wood, N. and Staniforth, A. 2002 Normal modes of deep atmospheres. Part I: Spherical geometry. *Q. J. R. Meteorol. Soc.*, **128,** 1771–1792?

Wallace, J. M., Tibaldi, S. and Simmons, A. 1983 Reduction of systematic forecast errors in the ECMWF model through the introduction of an envelope orography. *Q. J. R. Meteorol. Soc.*, **109,** 683–717

Wilson, D. R. and Ballard, S. P. 1999 A microphysically based precipitation scheme for the UK Meteorological Office Unified Model. *Q. J. R. Meteorol. Soc.*, **125,** 1607–1636